Computational Materials Physics
Project Team 1

Emile Segers
Ghent University, Department of Science: Physics and Astronomy

Maxim Torreele
Ghent University, Department of Engineering and Architecture: Engineering Physics

Victor Landgraf
T.U. Delft, Department of Chemistry

Wouter Heyvaert
University of Antwerp, Department of Physics
(Dated: December 3, 2020)

I. INTRODUCTION

In this paper we discuss the stability and phase transitions of γ'-Fe_4N as function of high pressures (up to 40GPa) by means of Density Functional Theory (DFT). To do this, we first discuss the reasoning behind our choice of input parameters for our DFT code of choice, which is Quantum Espresso [1, 2], in section II. Next we discuss the stability and phase transitions of the γ'-Fe_4N structure by analyzing its $E(V)$-curve in sections III, IV and V. All this work is based on the work done by [3]. Finally, we elaborate on the work of [3] by first analyzing the magnetic properties of γ'-Fe_4N in section VI and by calculating its elastic properties in section VII.

II. CONVERGENCE TESTING OF THE γ'-Fe_4N CRYSTAL STRUCTURE

The first obstacle to face in this project is finding a suitable `cif`-file that represents the γ'-Fe_4N crystal structure. This can be found on [4]. The pseudopotentials were retrieved from the Quantum Espresso input generator from Materialscloud, available at `https://www.materialscloud.org/work/tools/qeinputgenerator`. By changing the number of points in the K-mesh, kinetic energy cutoff for wavefunctions (*ecutwfc*) and for charge densities (*ecutrho*) independently, it is possible to get a stable hydrostatic pressure and assume it has converged when fluctuations in the hydrostatic pressure are less then 1kbar. As shown in figure 1, this happens at the following values: $k = 9\times9\times9$, $ecutwfc = 140$Ry and $ecutrho = 7\cdot ecutwfc = 980$Ry.

In [3] a k-mesh of $10\times10\times10$ and $ecutwfc$ of 800eV = 58.79889412Ry is used. As expected the k-mesh is about the same for both applications because this depends on the given structure that is calculated. In contrast the $ecutwfc$ parameter is dependent of external values like the pseudopotentials and this gives the significant difference between the 2 studies.

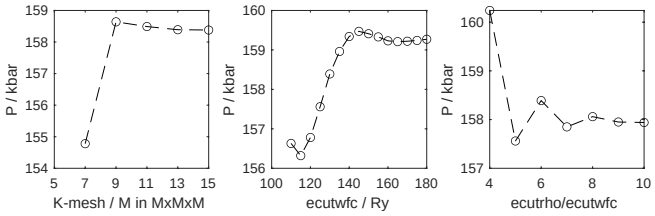

FIG. 1: Graphs of the hydrostatic pressure in function of K-mesh, ecutwfc and ecutrho. While testing each parameter, the other parameters were fixed at $k = 9\times9\times9$, $ecutwfc = 130$Ry, $ecutrho = 6\cdot ecutwfc$.

III. THE E(V)-CURVE FOR γ'-Fe_4N

The $E(V)$-curve can be calculated in two different ways. Since there is only one free parameter in the $Pm\bar{3}m$ crystal structure, namely the lattice parameter a, it is straightforward to choose different values for this single parameter to calculate the energy as a function of the volume. Another possible method is to use the `vc-relax` setting in Quantum Espresso. With this setting, a target pressure can be specified and the volume will be optimized to get the lattice parameter(s) that correspond to the given pressure. This is an iterative method which changes the lattice parameters and internal coordinates according to the forces acting upon the crystal. The difference between these two methods is that the latter will automatically find all the correct lattice parameters and internal coordinates, at the cost of longer computation times, whereas the first method requires manual geometry optimization at each volume where one wants to do a calculation. Because all members of our team have access to high performance computing, we opted for `vc-relax`.

Figure 2 shows the total energy versus the volume resulting from the `vc-relax` calculations. To find the equilibrium volume V_0, ground state energy E_0 and bulk modulus B_0, the Birch-Murnaghan Equation of States (EoS) was fitted to the calculated data. However, this EoS is only accurate up to $(1\pm0.1)V_0$, therefore only the

TABLE I: The results from the Pm$\bar{3}$m crystal structure for 0GPa, 10GPa and 30GPa, compared with the results for 0GPa and 10GPa mentioned in [3].

	Our results			Results from [3]		
Pressure (GPa)	a (Å)	V (Å^3)	$\frac{V_0-V}{V_0}$ (%)	a (Å)	V (Å^3)	$\frac{V_0-V}{V_0}$ (%)
0	3.792	54.54	0.0	3.795	54.66	0.0
10	3.711	51.12	6.3	3.705	50.86	7.0
30	3.610	47.06	13.7			

values that are within this range were used to fit the EoS. We find an equilibrium volume of $V_0 = 54.54$Å^3, with a ground-state energy of $E_0 = -1337.29201$Ry and a bulk modulus $B_0 = 178.8$GPa.

Our results are compared with those from [3] in table I. Here, the lattice parameter a and the volume $V = a^3$ are given for different pressures. Also the relative volume reduction is given. This property is defined by $\frac{V_0-V}{V_0}$, where V_0 is the volume at 0GPa. We observe that the equilibrium volume only deviates 0.12Å^3 from the value given by [3]. Such small deviations can be caused by using different DFT codes, or even by the margin of error that is inherent to using iterative methods that work with a threshold to stop their iterations. We conclude that the equilibrium values are in good correspondence with the values in [3].

IV. THE M-INSTABILITY

In [3] can be seen that γ'-Fe_4N has imaginary frequencies in the phonon spectrum at the M-point at a pressure of 10GPa. This indicates that there will be a phase transition between 0GPa and 10GPa to a crystal structure with lower symmetry. The new low-symmetry crystal structure can be found by analyzing this so-called soft-mode. This has been done in [3] and results in a P2/m crystal structure.

It can be shown that this structure arises due to a particular phonon in the M-point. To do so, one makes use of the `ISODISTORT`-tool, available on `https://stokes.byu.edu/iso/isodistort.php`. When the `cif`-file of the original Pm$\bar{3}$m structure is loaded onto this platform, a whole range of possible phonons is shown. Now one can identify a mode that yields a transition to a P2/m structure, which is indeed present at the M-point (it is an M5-phonon to be exact). Finally, if the right amplitudes for the displacive modes and the strains are filled out, it is possible to construct the new P2/m configuration. This method of finding a new low-symmetry crystal structure will be further elaborated upon in section V, where we analyze the X-instability at 30GPa.

We created a `cif`-file based on the information in table 2 from [3] which we then used for our calculations. The same kinetic energy cutoffs were used, but the K-mesh was changed to $7 \times 9 \times 7$ to keep the K-point density similar to that used for the high-symmetry crystal structure. We then used the same `vc-relax` method as described earlier in chapter III to create an $E(V)$-curve for this low-symmetry crystal structure. The results can be found in figure 2. Also here we fitted the Birch-Murnaghan EoS to the datapoints in a range of ±10% around the equilibrium volume. From that fitted EoS we derive an equilibrium volume of $V_0 = 108.84$Å^3, along with the equilibrium energy $E_0 = -2674.58378$Ry and bulk modulus $B_0 = 162.5$GPa. To compare these values with those found for the Pm$\bar{3}$m crystal structure, we divide these values by the number of formula units in the unit cell, which is two for the P2/m crystal and 1 for the Pm$\bar{3}$m crystal. Thus we find E_0/f.u. $= -1337.29189$Ry for the low-symmetry structure, this is higher than the ground-state energy for the high-symmetry structure, indicating that the high-symmetry structure is indeed the more stable structure at 0GPa.

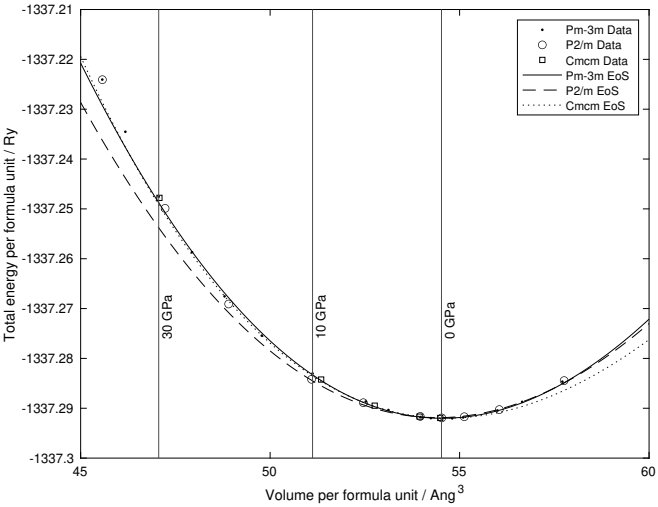

FIG. 2: The $E(V)$-curve for the Pm$\bar{3}$m, P2/m and Cmcm crystal structures. The Birch-Murnaghan EoS was fitted to the datapoints within a range of ±10% of the equilibrium volume for all structures. The volumes that correspond to pressures of 0GPa, 10GPa and 30GPa for the Pm$\bar{3}$m crystal structure are marked by vertical lines. The other two structures reach the same pressures at approximately the same volumes.

By further inspection of our results in figure 2, we see that there is a crossover of the two equations of state between 0GPa and 10GPa. Therefore, the P2/m crystal structure is more stable than the original high-symmetry

TABLE II: The resulting space group and total energy of the candidate structures at 30GPa after full relaxation.

Phonon	Space group	$E/f.u.$ at 30GPa (Ry)
X1+P1	P4/mmm (123)	-1337.08657
X1+P5	Cmcm (63)	-1337.24777
X2+P1	P42/mmc (131)	-1337.24660
X5+P2	Pmma (51)	-1337.16718
X5+C5	P21/m (11)	-1337.16717

structure for higher pressures. However, as we mentioned earlier already, the EoS is only accurate up to ±10% of the equilibrium volume, which can be clearly observed in figure 2. Namely, according to the EoS the low-symmetry crystal will stay more stable for a very large pressure range, but in our calculations we observe that the high-symmetry crystal structure will again reach lower energies around 40GPa. The P2/m structure is thus only the more stable configuration in a range between 0GPa and 40GPa. This conclusion is confirmed by [3].

V. THE X-INSTABILITY

The 30GPa phonon dispersion of γ'-Fe_4N ($Pm\bar{3}m$) displays a soft mode at the X-point [3]. This suggests that the $Pm\bar{3}m$ structure is not stable at this pressure [5]. The wave vector and the irreducible representation of the soft mode can be used to identify candidate stable phases [5]. We used the `ISODISTORT` tool from the `ISOTROPY` [6] software suite to generate 'first guesses' of the candidate structures which were then further relaxed, allowing all degrees of freedom to relax. We could derive a long list of structures from the soft mode, from which we analyzed the 5 structures listed in table II.

The Cmcm candidate has the lowest total energy at 30GPa, and this energy is indeed lower than the total energy of γ'-Fe_4N at that pressure (-1337.24754Ry). However, it is less stable than the P2/m structure, which emerges from the soft mode at 10GPa (figure 2). Our findings thus suggest that the P2/m structure is the most stable structure at 30 GPa. However, it could be that the most stable structure was not found, because we only investigated 5 structures from all the possibilities. On top of that, the quest for configurations could be continued by calculating the phonon dispersion of all the resulting structures. Soft modes in these structures may reveal other candidates that may be more stable than the P2/m structure. '

VI. MAGNETISM

In this first elaboration, an attempt is made to physically explain the occurrence of soft modes of the original structures. Most of this reasoning is based upon [3], but it is a nice check and gives some physical insight into the phase transition at 10GPa. Fig. 3a shows our own results of the magnetic moment per site. The N-atoms clearly do not contribute to the total magnetic moment of the unit cell. A more detailed calculation in [3] points out that this magnetism arises due to the 3d electrons of iron. The magnetic moment of the iron atoms at the face centers of the unit cell seems to decrease with increasing pressure, whereas the magnetic moment of the corner iron atoms remains more or less the same. Since the iron atoms at the face centers are closer to the central nitrogen atom, this effect is prescribed to the presence of that interstitial atom. The increase in pressure leads to a redistribution of electric charge and, thus, a change in magnetic moment.

The phenomenon of magnetostriction suggests that there exist tight links between the stability of the phonon spectrum and the magnetic moment. Magnetization of the structure results in a lattice dynamical equilibrium situation of the structure: the N-atom is held stationary by the present magnetic field. When the pressure applied on the structure increases, the magnetic moment tends to disappear as stated above. So one may say that the pressure removes the stabilizing effect of the magnetic fields. Due to this disturbance of the inter-atomic interactions, soft modes can appear in the phonon spectrum, which indicates the instabilities. This is the case at the M-point of the first Brillouin zone for a pressure of 10GPa. Now it is interesting to use the soft mode method to obtain a new structure that is more stable at this pressure than the original one. The result is a P2/m configuration, of which an entire analysis can be found in Section IV.

It can now be examined how the stability of the new-found structure is reflected in its magnetic properties. Therefore, the total magnetic moment per formula unit as a function of pressure is displayed in Fig. 3b. A first observation is that this curve shows a much steeper descent for the P2/m structure than for the original structure. Following the above reasoning, the latter is the more stable crystal. But for further increasing pressure, the original structure undergoes a fast decrease in magnetic moment, whereas the new structure goes down at a smaller rate. This could point towards the fact that the P2/m structure becomes more favorable around this pressure. We note that in the findings of [3], the magnetic moment of the P2/m structure is actually lower than that of the initial structure. This small difference can be explained by the use of different DFT codes.

VII. ELASTIC PROPERTIES

In order to elaborate further on the structure given in [3], we computed the elastic constants. To do so, we made use of the stress-strain method. In general, the input parameters remain identical to those used in Section III, except that we are executing SCF-calculations with a slightly more dense K-mesh of $13\times13\times13$. This increases

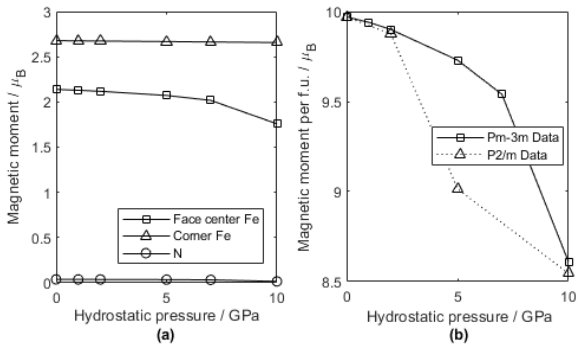

FIG. 3: The magnetic moment present at the corresponding sites in the $Pm\bar{3}m$ structure (a) and a comparison of the total magnetic moment per formula unit between $Pm\bar{3}m$ and P2/m (b).

TABLE III: The elastic properties of γ'-Fe_4N from our calculations and the Materials Project database.

	Our results	Results from [4]
Bulk modulus K_V (GPa)	187	193
Shear modulus G_V (GPa)	49	61
Young's modulus (GPa)	136	165
longitudinal speed of sound ($\frac{m}{s}$)	5918	5875
shear speed of sound ($\frac{m}{s}$)	2615	2770

the accuracy. Furthermore, the six independent deformation gradients as recommended in the course notes are considered (Part C: 9. elasticity). These calculations are performed twice: once for $\delta_1 = 0.01$ and $\delta_2 = 0.03$, and once for $\delta_1 = -0.01$ and $\delta_2 = -0.03$. In the end, the total matrix of elastic constants C is computed as the average of these two cases, with the aim of reducing numerical noise.

A formula for the elastic constants is given in the course notes, namely

$$\boldsymbol{\sigma} = C\boldsymbol{\epsilon},$$

with $\boldsymbol{\sigma}$ the stress tensor in Voigt notation, $\boldsymbol{\epsilon}$ the strain tensor in Voigt notation and C the elastic constants. Using this notation, we obtain $C_{11} = 291$GPa, $C_{12} = 135$GPa and $C_{44} = 31$GPa for our cubic unit cell. A first observation that can be made consists of checking whether these elastic constants meet the Born stability criteria. As $C_{11} > 0$, $C_{44} > 0$ and $C_{11} > C_{12}$, this is indeed the case, from which follows that the system in this regard is stable. Based on these constants, it is also possible to compute several elastic moduli. These are shown in table III. To check our results, they are compared to data from the Materials Project database [4]. An explanation for the deviation between the two is partly explained by the use of a different lattice parameter. Overall, they are in fair agreement. The bulk modulus is also relatively close to the one calculated in Section III, although both were derived using different techniques. As a final step, the speed of sound in the longitudinal and shear direction is calculated and shown in table III as well. We can see that those are typical values for the speed of sound in solids [7].

VIII. CONCLUSION

In this paper we were able to reproduce most of the findings described in [3]. More specifically we were able to reproduce the $E(V)$-curve for γ'-Fe_4N (section III) and the phase transition to a P2/m crystal structure due to the M-instability at 10GPa (section IV). For the X-instability (section V) we tried finding an alternative structure that is more stable at 30GPa but none of the candidate structures that we examined had a low enough total energy From our calculations, we conclude that the P2/m structure remains the most stable configuration. At last we took a look at the magnetic (section VI) and elastic (section VII) properties at different pressures which concurred with [3] and [4].

[1] P. Giannozzi *et al.*, "Advanced capabilities for materials modelling with Quantum ESPRESSO," *Journal of Physics: Condensed Matter*, vol. 29, p. 465901, nov 2017.

[2] P. Giannozzi *et al.*, "QUANTUM ESPRESSO: A modular and open-source software project for quantum simulations of materials," *Journal of Physics Condensed Matter*, vol. 21, p. 395502, sep 2009.

[3] T.-m. Cheng, G.-l. Yu, Y. Su, L. Zhu, and L. Li, "Spontaneous magnetization-induced phonons stability in γ-Fe4N crystalline alloys and high-pressure new phase," *Journal of Magnetism and Magnetic Materials*, vol. 451, pp. 87–95, 2018.

[4] K. Persson, "Materials data on Fe4N (sg:221) by materials project," 2 2016. `https://materialsproject.org/materials/mp-535/`.

[5] Y. K. K. Parlinski, "Ab initio study of phonons and structural stabilities of the perovskite-type MgSiO3," *The European Physical Journal B*, vol. 16, pp. 49–58, 2000.

[6] D. E. T. D. M. H. B. J. Campbell, H. T. Stokes, "ISODISPLACE: An Internet Tool for Exploring Structural Distortions.," *Journal of Applied Crystallography*, vol. 39, pp. 607–614, 2006.

[7] M. L. Williams, "CRC Handbook of Chemistry and Physics David R. Lide," 1996.